

BMRI TISEHHT: Brain MRI Image Segment Based On Enhanced Hilbert Huang Transform

¹VijayaLakshmi S and ²Padma S

¹*Assistant Professor, Faculty of Electronics and Communication Engineering
Sona College of Technology, Salem
vijayalakshmis0783@gmail.com*

²*Professor, Department of Electrical and Electronics Engineering,
Sona College of Technology, Salem, Tamilnadu*

Abstract

We present a method for brain tissue segmentation from Magnetic Resonance Images (MRI) with the help of Enhanced Hilbert Huang Transform. Segmentation of medical imagery is a challenging problem due to the complexity of the images, as well as to the absence of models of the anatomy that fully capture the possible deformations in each structure. To perform the normal and pathological tissue segmentation, the brain MRI is need to classified. Hence in this paper, classification is done with the help of Feed Forward Back Propagation Neural Network (FFBNN) and Fuzzy Logic classifiers. After the classification, the normal tissues like White Matter (WM), Grey Matter (GM) and Cerebrospinal Fluid (CSF) are segmented from the normal BMRI. Pathological tissues like Tumor and Edema are segmented from the abnormal BMRI. Both the classification and the segmentation performance of the proposed technique are evaluated in terms of accuracy, sensitivity and specificity. The implementation result shows the efficiency of proposed tissue segmentation technique in segmenting the tissues accurately from the BMRI.

Keywords: Feed Forward Back Propagation Neural Network (FFBNN), Enhanced Hilbert Transform (EHHT), Fuzzy Logic, Tissue Segmentation,

1. Introduction

The brain is the anterior most part of the central nervous system. Along with the spinal cord, it forms the Central Nervous System (CNS). The Cranium, a bony box in the skull protects it. Virtually everything we do, think, act, reason, walk, talk, the list is endless is because of our brain.

Brain Tumors are one of the diseases caused in the brain. Tumor is an abnormal growth caused by cells reproducing themselves in an uncontrolled manner. A benign brain tumor consists of benign (harmless) cells and has distinct boundaries. Surgery alone may cure this type of tumor. A malignant brain tumor is life-threatening. It may be malignant because it consists of cancer cells, or it may be called malignant because of its location. A malignant brain tumor made up of cancerous cells may spread or seed to other locations in the brain or spinal cord. It can invade and destroy healthy tissue so it cannot function properly. The structure and function of the brain can be studied noninvasively by doctors and researchers using Magnetic Resonance Imaging (MRI). The MRI image is actually a thin horizontal slice of the brain. The white area at lower left is the tumor. It looks white because MRI scans enhance tissue differences. The tumor is actually on the right side of the brain.

Recently, many people use the MRI data to research the relation between white matter development and neural diseases, especially, the anatomy image is fusing with those images from diffusion tensor imaging, and using the white matter to lead the fibre track [1-2], the accuracy of segmenting white matter is key problem. Attention deficit hyperactivity disorder (ADHD) [3] is also needed to segment white matter. In spite of many algorithms for segmenting MRI of data [4-8], such as watershed algorithm, eSneke algorithm, genetic algorithm. In addition, those algorithms are based on the homogeneity of image. In fact, intensity inhomogeneity is impact on every image and we have to solve the problem with new method. Wells [9] developed a new statistical approach based on the expectation-maximization (EM) algorithm, but the results are too dependent on the initial values, extremely consuming the time and just looking for local maximum point.

The basic goal in segmentation process is to partition an image into regions that are homogeneous with respect to one or more characteristics [10]. Segmentation is an important tool in medical image processing and it has been useful in many applications, such as: detection of tumors, detection of the coronary border in angiograms, surgical planning, measuring tumor volume and its response to therapy, automated classification of blood cells, detection of micro calcifications on mammograms, heart image extraction from cardiac cine angiograms, etc [11]-[14]. In some applications, it may be useful to classify image pixels into anatomical regions, such as bones, muscles, and blood vessels, while in others into pathological regions, such as cancer, tissue deformities, and multiple sclerosis lesions. In magnetic resonance (MR) images processing, the goal is to divide accurately the entire image into sub regions included gray matter (GM), white matter (WM) and cerebrospinal fluid (CSF) spaces of the brain [15]. For example, in a number of neurological disorders such as multiple sclerosis (MS) and Alzheimer's disease, the volume changes in total brain, WM, and GM can provide important information about neuronal and axonal loss [16].

In recent years, many algorithms have been proposed for brain MRI segmentation. The most popular methods are included thresholding [8], region-growing [9], and clustering. The full automated intensity-based algorithms have high sensitivity to various noise artifacts such as intra-tissue noise and inter-tissue intensity

contrast reduction. Thresholding is very simplicity and efficiency. If the target is clearly discernible from background, the intensity histogram of the image is bimodal and it can easier get to the optimal threshold by simply choosing the valley bottom as the threshold point. However, in most of real images, there are not clearly discernible marks between the target and the background. Clustering is most popular approach for segmentation of brain MR images and typically performs better than the other methods [10].

The rest of the paper is organized as follows: Section 2 reviews the related works with respect to the proposed method. Section 3 discusses about the proposed technique. Section 4 shows the experimental result of the proposed technique and section 5 concludes the paper.

2. Literature survey

A lot of researches have been proposed by researchers for the brain image segmentation. A brief review of some of the recent researches is presented here.

Arnaldo Mayer and Hayit Greenspan [20] presented an automated segmentation framework for brain MRI volumes based on adaptive mean-shift clustering in the joint spatial and intensity feature space. The method was validated both on simulated and real brain datasets, and the results were compared with state-of-the-art algorithms. The advantage over intensity based GMM EM schemes as well as additional state-of-the-art methods was demonstrated. They also showed that using the AMS framework, segmentation of the normal tissues is not degraded by the presence of abnormal tissues. Although only a rudimental bias field correction step implemented and no spatial prior is extracted from an atlas, the algorithm gave good results on noisy and biased data thanks to the adaptive mean-shift ability to work with non-convex clusters in the joint spatial intensity feature space as well as the mean-shift noise smoothing behavior. In future research, they examined ways to improve the current algorithm's limitations. In particular, the current bandwidth selection algorithm based on the k-nearest neighbor makes no use of application specific information. Edge information, for instance, helped define the region of influence of a kernel by a given point since edges generally delimit regions corresponding to different tissue types. More-over, the scalar bandwidth considered in proposed work replaced by a full bandwidth matrix that better captures local structures orientation.

Mert R. Sabuncu et al. [21] investigated a generative model that leads to label fusion style image segmentation methods. Within the proposed framework, they derived several algorithms that combine transferred training labels into a single segmentation estimate. With a dataset of 39 brain MRI scans and corresponding label maps obtained from an expert, we empirically compared these segmentation algorithms with Free Surfer's widely-used atlas-based segmentation tool. Their results demonstrated that the proposed framework yields accurate and robust segmentation tools that employed on large multi-subject datasets. In a second experiment, they employed one of the developed segmentation algorithms to compute hippocampal volumes in MRI scans of 282 subjects. A comparison of these measurements across clinical and age groups indicate that the proposed algorithms were sufficiently

sensitive to detect hippocampal volume differences associated with early Alzheimer's Disease and aging.

Feng Shi et al. [22] have presented a framework for performing neonatal brain tissue segmentation by using a subject-specific tissue probabilistic atlas generated from longitudinal data. Proposed method has taken the advantage of longitudinal imaging study in their project, i.e., using the segmentation results of the images acquired at a late time to guide the segmentation of the images acquired at neonatal stage. The experimental results demonstrated that the subject-specific atlas has superior performance, compared to the two population-based atlases, and also the proposed algorithm achieves comparable performance as manual raters in neonate brain image segmentation. The atlas sharpness parameter has been proved robust form achieving optimal segmentation results in a broad range of 0.3–0.6. For the selection of late time-point image, the segmentation accuracy remains similar when the atlas was built by either one-year-old or two-year-old image. Recently, decision fusion was widely used to combine multiple segmentations into a final decision with compensation for errors in single segmentation.

Juin-Der Lee et al. [23] presented the most statistical segmentation methods in the literature have assumed that either the intensity distribution of each tissue type was Gaussian, or the logarithmic transformation of the raw intensity was Gaussian. However, the manual segmentation results provided by the IBSR suggested that intensity distributions of brain tissues can be varying asymmetric and non-Gaussian. Instead of setting up additional classes to model "mixels," they proposed a power transformation approach to perform automatic segmentation of brain MR images into CSF, GM, and WM. It was intuitively clear that the well-known Box-Cox power transformation model was able to provide a statistically meaningful and useful solution to proposed problem. The shape parameter used to extend traditional Gaussian mixture models further to encompass not only Gaussian intensity distributions but also non-Gaussian distributions. The parameters and can be estimated using the EM algorithm. They validated the approach against four real and simulated datasets of normal brains from the IBSR and Brain Web. Any preprocessing bias-field correction method (e.g., N3 or 3-D wavelet-based bias correction) can be easily incorporated into a pipeline framework for the pro-posed method. Experiments on real data from the IBSR have indicated that the proposed approach achieves higher Jaccard indexes compared with other methods currently in use. The power transformation approach not only preserves the simplicity of the Gaussian mixtures, but also has the potential to generalize to multivariate versions adapted for segmentation using multi-modality images.

Dalila Cherifi et al. [24] described normal tissue's recognition then tumor extraction (applied for GBM and MS diseases). They have presented brain recognition methods to separate the abnormal tissues. They have proposed and applied method based on thresholding used for tumor extraction (GBM and MS diseases). They have found that the local thresholding gives a good results comparing with the others. We conclude that when we combine median filter, local thresholding and post processing in such way that the resultant algorithm is more robust. As a general method, they have implemented classification based on EM segmentation method for both; tissue

recognition and tumor extraction. Proposed method given us better results when they compared it with thresholding specially for detecting the small regions of necrotizing tissue which was inside Anaplastic cells (pseudo-Palisading necrosis) for GBM tissue; it mainly because of parameters that used in this algorithm. As the further work, it was interesting to study other tumors types, especially those that have characterized similar to the GBM and MS diseases studied there and could be considered in the use of multi-resolution Gaussian expectation maximization to characterize tumors. With MRI, it was possible to confirm the presence and extent of the lesion and, by processing the images with computers, valuable information can be obtained.

Nagesh Vadaparathi et al. [25] presented a paper in which particular cases such as Acoustic neuroma, it was assumed that there was a possibility of hearing loss, dizziness and other symptoms related to brain. Some acoustic neuromas can be treated with surgery. Therefore, it needed to segment the image more accurately, which helped to identify the damaged tissues to be repaired and can be corrected by surgery. Hence, in proposed paper, a new novel segmentation algorithm based on Skew Gaussian distribution proposed which helped to identify the tissues more accurately. Due to the basic structure of Skew Gaussian distribution, it was well suited for both symmetric as well as asymmetric distribution. The performance evaluation carried out by using quality metrics. The results showed that, proposed developed algorithm outperforms the existing algorithm. Many models were utilized to identify the diseases, but MRI brain segmentation has gained popularity over the other models because of the non-ionizing radiation that was used.

3. Proposed Brain MRI Image classification and Tissue classification

Here a new technique is proposed to classify the Brain Magnetic Resonance Images (BMRI) and performs the tissue segmentation. Initially, the features such as correlation and covariance are extracted from the input BMRI, which are obtained from the database. Soon after, the extracted features are fed as the input to the FFBNN and Fuzzy classifier to classify the BMRI. Subsequently, the classified abnormal BMRI are applied to Enhanced Hilbert Huang Transform (EHHT) for segmenting the abnormal tissues such as Tumor, Edema from the abnormal BMRI. While the normal BMRI tissues such as White Matter (WM), Gray Matter (GM) and Cerebrospinal Fluid (CF) are segmented from the normal BMRI. Architecture of the proposed Brain MR Image tissues segmentation technique is given in figure1.

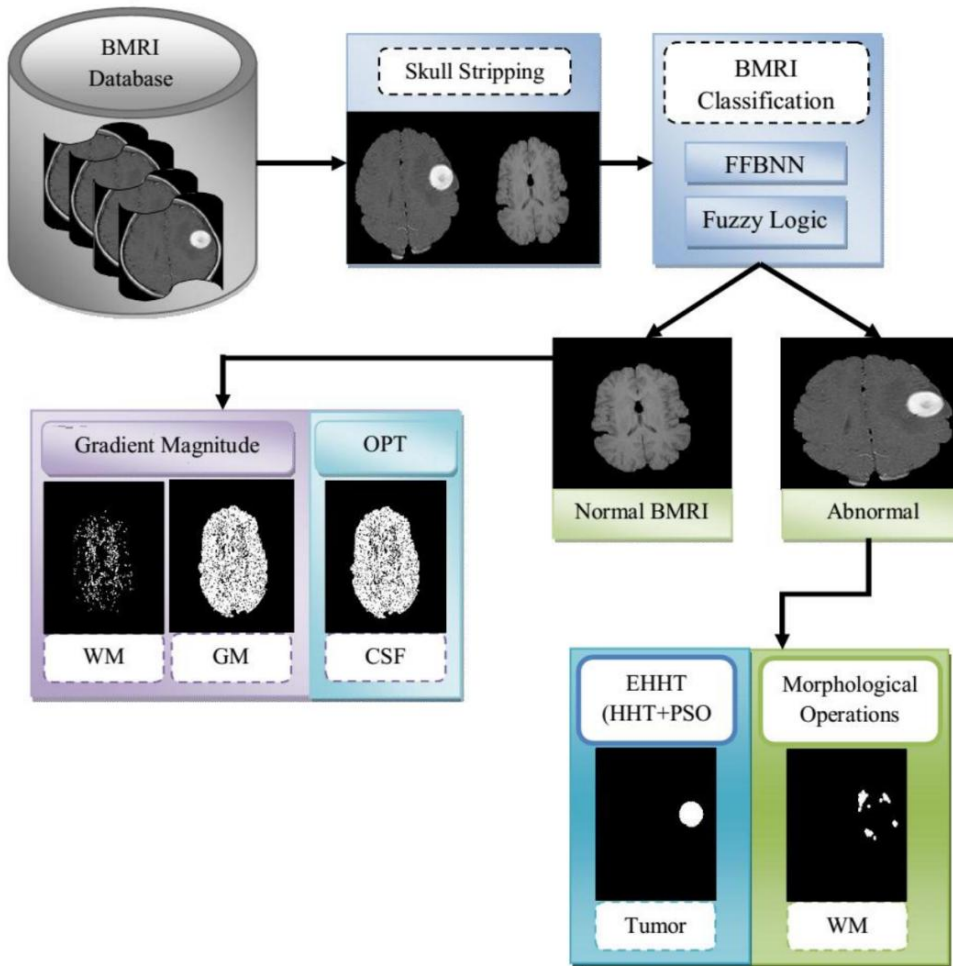


Figure1. Architecture of the proposed Tissue Segmentation Technique

The proposed technique consists of the following stages:

- ❖ Feature Extraction
- ❖ Classification using FFBNN and Fuzzy
- ❖ Segmentation using EHHT-PSO

3.1) Skull Stripping

Let the database (D) which consists of BMRI and $I_{x,y}$ be the one of the MRI brain images has the size of $(m \times n)$ taken from the database as the input where $x \in 1, 2, \dots, m$ and $y \in 1, 2, \dots, n$. Generally, skull-stripping is the procedure employed to segregate the skull from the MR images of the brain region. It divides the brain from the skull and other surrounding brain segments. The fundamental objective skull-stripping is the elimination of the scalp, skull and dura segments in the brain. The measures taken to segregate the skull from the Brain images are detailed below.

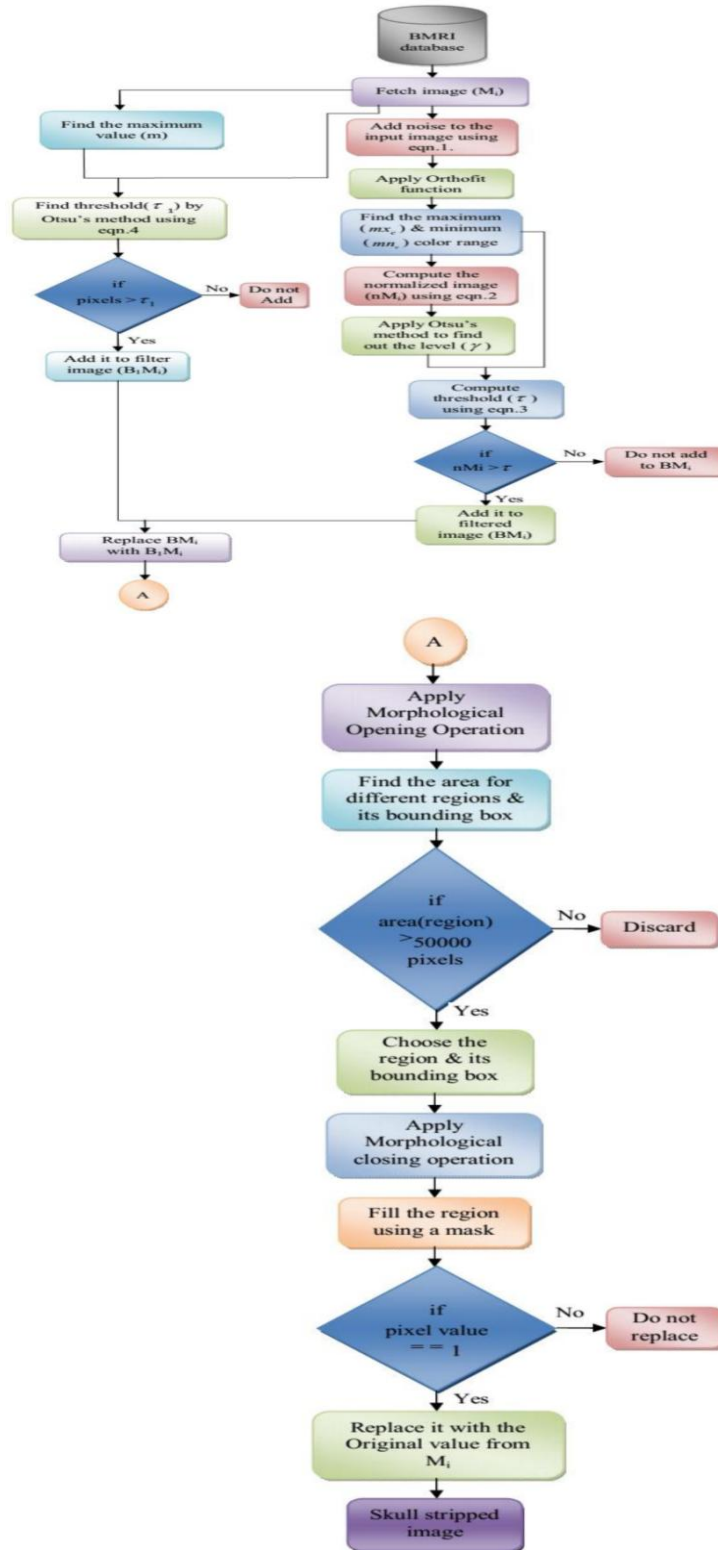


Figure 2: Process of Skull Stripping

Initially, the input BMRI (M_i) is fetched from the BMRI database (D). After that noise is added to M_i by using the following equation 1.

$$NM_i = \sin(M_i^3 / 100)^2 + \frac{1}{20} \times \text{rand}(\text{size of } M_i) \quad (1)$$

Where,

NM_i - Noise added Image

After that, orthofit function is applied on M_i and NM_i and the resultant image is denoted as OM_i . Next to that the maximum valued pixel (m) from the input image (M_i) and the limit ($\max(mx_c)$ & $\min(mn_c)$) of the colour range exists on the image OM_i are predicted. Then the image obtained while applying orthofit function is normalized as in equation (2) which utilizes the limits (mx_c) & $\min(mn_c)$ and OM_i and denoted as (nM_i)

$$nM_i = (OM_i - mx_c) / (mx_c - mn_c) \quad (2)$$

After computing the normalized image (nM_i), normalized level (γ) is calculated by applying the familiar Otsu's technique on nM_i . With the help of the calculated normalized level (γ) and the colour range limits, threshold (τ) is computed as in equation (3).

$$\tau = \gamma \times (mx_c - mn_c) + mn_c \quad (3)$$

Subsequently, the pixels values in the (nM_i) is compared with the threshold (τ) and the pixels greater than the threshold (τ) is added to a filter image represented as (BM_i). As in equation (4), threshold (τ_1) is computed which exploits the Otsu's method and the maximum valued pixel (m).

$$\tau = \text{Otsu}'s \left(\frac{M_i}{m} \right) \times m \quad (4)$$

Here also τ_1 is compared with the M_i and the pixels greater than τ_1 are added to the filtered image named as B_1M_i . Following that BM_i is replaced by means of B_1M_i . The resultant image is subjected to the opening operation of morphological operator using MATLAB function `imopen()`. Then area and the bounding box are calculated for each region existing in the image obtained after

applying morphological operation where bounding box is nothing but the pixels present in the edges of each region. The region at which the area is greater than 50000 pixels is selected with its corresponding bounding box. Then closing operation of morphological operator using MATLAB function `imclose()` is applied on the selected region. After that, a mask with size of $w \times w$ is created and using that mask, the selected region is filled within its corresponding bounding box. The pixels which are having value one and its corresponding position are find out and that positions are replaced with the original value corresponding to that position taken from M_i . The resultant image (I_i) is the skull stripped image and it is used for feature extraction.

3.1 Feature Extraction

The calculation of the covariance C_o and correlation C_r are given below in the equations 5 and 6.

$$C_o = \frac{1}{mn} \sum \left(I(x, y) - \left(\frac{1}{mn} \sum_{x=1}^m \sum_{y=1}^n I(x, y) \right) \right) \quad (5)$$

$$C_r = \frac{C_o}{\sqrt{\left(\frac{1}{mn} \sum_{x=1}^m \sum_{y=1}^n \left(I(x, y) - \left(\frac{1}{mn} \sum_{x=1}^m \sum_{y=1}^n I(x, y) \right) \right)^2 \right)}} \quad (6)$$

Where,

m - number of rows of the given input image

n - number of columns of the given input image

These calculated correlation and covariance features are given to the FFBNN and Fuzzy Classifier to classify the BMRI.

3.2 Classification using FFBNN

In order to detect whether the given BMRI is abnormal or normal, Feed Forward Back Propagation Neural Network (FFBNN) [27] is utilized and it is trained using the covariance C_o and correlation C_r values extracted from each and every image in the database. The extracted features are given to neural network for training and classification purpose. The neural network is well trained using these extracted features. The neural network consists of 2 input units, h hidden units and one output unit. The structure of the FFBNN is given as below:

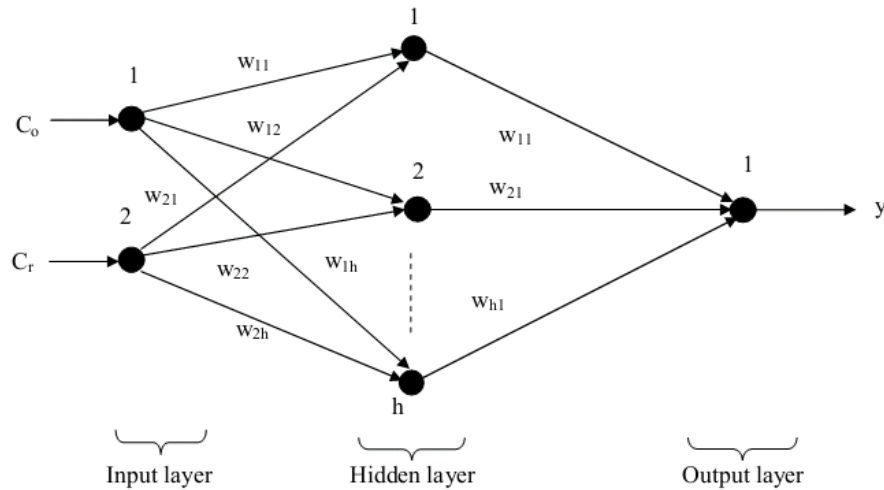


Figure3. Diagram of the FFBNN

3.3 Classification using Fuzzy

Fuzzy Rule based classification is a method of generating a mapping from a given input to an output using fuzzy logic. Then, the mapping gives a basis, from which decisions can be generated. Membership Functions, Logical Operations, and If-Then Rules are used in the Fuzzy Rule based Process. The Stages of Fuzzy are,

- 1) Fuzzification
- 2) Fuzzy Rules Generation
- 3) Defuzzification

3.3.1. Fuzzification

During the fuzzification process, to convert the crisp input in to linguistic variables are converted in to fuzzy. For the fuzzification process, the inputs are covariance σ_0 and correlation σ_r values extracted from the skull stripped BMRI.

3.3.2. Fuzzy Rules Generation

According to the fuzzy values for each feature that are generated in the Fuzzification process, the Fuzzy Rules are also generated. The rules are in the form of “IF A THEN B”

The “IF” part of the Fuzzy Rule is called as “antecedent” and also the “THEN” part of the rule is called as “conclusion”.

3.3.3. Defuzzification

The input given for the Defuzzification process is the fuzzy set and the output obtained is a single value, y_1 or y_2 for a given BMRI image. From this value, we can able to classify whether the given input BMRI image is normal or abnormal. The Fuzzy is trained with the use of the Fuzzy Rules and the testing process is done with the help of datasets.

3.4 Segmentation of classified tissues

The classified BMRI images by means of FFBNN and Fuzzy Classifier are applied to segment the normal and abnormal tissues. From the normal BMRI, the normal tissues like White Matter (WM), Gray Matter (GM) are segmented with the help of Gradient technique and Cerebro-Spinal Fluid (CSF) is segmented using OPT and abnormal tissues like tumor and edema are segmented from the abnormal BMRI using EHHT. The segmentation procedure of both abnormal and normal tissues is explained in the following sections.

3.4.1 Segmentation of WM and GM using Gradient Technique

For segmenting the White Matters and Gray Matters, the normal BMRI obtained after the classification I_N is subjected into gradient technique. The Gaussian Convolution filter that utilized in this technique makes the image I_N into smoothed image I_{NS} . After that, the smoothed image I_{NS} is subjected with Gradient operation. The gradient of two variables x and y are specified as follow:

$$\nabla I_{NS}(x, y) = \frac{\partial I_x}{\partial x} \hat{e} + \frac{\partial I_y}{\partial y} \hat{f} \quad (7)$$

The gradient values are useful to mark the current edges in the image that are specified in the following equations (8) and (9).

$$S = x_{(e)}^2 + y_{(f)}^2 \quad (8)$$

$$EM = \frac{1}{(1 + S)} \quad (9)$$

The process of Binarization is then carried out on the edge marked image EM . In this Binarization procedure, the value of gray level of every pixel in EM image is estimated by means of a global threshold value τ . The resultant binarized image after the Binarization process is I_{NB} .

By use of Morphological Opening and Closing operation, the small holes and small objects from the image I_{NB} is eliminated. Currently, in our work, the WM and GM normal tissues of normal BMRI images are segmented by means of the intensity values.

$$I_{WG} = \begin{cases} WM, & \text{if } I_{NB_i} = 1 \\ GM, & \text{if } I_{NB_i} = 0 \end{cases} \quad (10)$$

The exacting part is segmented into White Matter, if the intensity value of the image part is one and then it is considered as Gray Matter part, if the intensity value is zero, and subsequently the images are segmented according to the equation (10).

3.4.2 Segmentation of CSF by means of OPT

CSF tissue from the image I_N is segmented by Orthogonal Polynomial Transform (OPT) using the formula given below:

$$I_{CSF} = \text{Sin} \left(\frac{I_{N(i)}^3}{100} \right) + 0.05 * \text{rand}(|I_N|) \quad (11)$$

At present, the CSF tissue I_{CSF} from the normal image is segmented efficiently. Therefore, the normal tissues WM, GM and CSF are segmented from the skull stripped image I_N .

3.4.3 Exploitation of EHHT for Segmenting Tumor Tissues

The images classified as abnormal BMRI are obtained and given to EHHT to segment the abnormal tissues such as tumor and edema separately. EEHT is a combination of HHT and PSO.

3.4.3.1 Hilbert Huang Transform

By employing Empirical Mode Decomposition (EMD) [30] the tumor tissues are segmented. N. Huang [29] recently introduced a technique that decomposes a signal into a sum of components, each with slowly varying amplitude and phase. Once one has a signal represented in such a form, using the Hilbert Transform one may analyze the properties of each component. Every component of the EMD is called an Intrinsic Mode Function (IMF). The two criteria will satisfy the IMFs, as modes, so that they will resemble a generalized Fourier decomposition.

1. In the whole dataset, the number of extrema and the number of zero-crossings must either equal or differ at most by one, and
2. At any point, the mean value of envelope defined by the local maxima and the envelope defined by the local minima is zero.

More specifically, a real valued input signal is represented by $X(k)$, and then the application of EMD generates a set of M IMFs $IMF_j(k)$, $j=1, \dots, M$, such that

$$X(k) = \sum_{j=0}^M IMF_j + res(k) \quad (12)$$

Where the residual $res(k)$ is a monotonic function and it represents the trend within the original signal. The following algorithm gives the method that is used for the extraction of IMF from the signal $x'(k)$.

1. The set of IMFs is initially defined as $M = \phi$ (empty set).
 2. Find the locations of all extrema of $x'(k)$.
- a) $x'(k) = X - \sum_{i \in I} IMF_i$

- b) Compute k^{th} IMF (sifting).
- i) Interpolate (using cubic spline interpolation) between all the minima (resp. maxima) to obtain the signal envelope passing through the minima $e_{\min}(k)$ (resp. $e_{\max}(k)$).
- ii) Compute the local mean of these envelopes $m(k) = \left(e_{\min}(k) + e_{\max}(k) \right) / 2$.
- iii) Subtract $x'(k)$ from the mean $m(k)$ to obtain the oscillating signal $s(k) = x'(k) - m(k)$.
- iv) If the resulting signal $s(k)$ obeys the stopping criterion, $IMF(k) = s(k)$ becomes IMF.
- v) Otherwise set $x'(k) = s(k)$ and repeat the process from steps i to v.
- c) $x'(k)$ is added to set M .

The stoppage criterion used in the final step can be, for instance, the normalized squared difference between two successive sifting iterates $s_{pre}(t)$ and $s_{cur}(t)$, that is

$$SD = \sum_{t=0}^T \left[\frac{\left| s_{pre}(t) - s_{cur}(t) \right|^2}{s_{pre}(t)} \right] \tag{13}$$

Where T represents the total number of samples in the original series, and the empirical value of SD is using a set within the range (0.2-0.3). Upon obtaining an IMF, the same procedure is applied to the residual signal $res(k) = x'(k) - IMF(k)$ to extract the next IMF. The process is continued until all the IMFs are extracted and no other oscillations are carried in the remaining signal, illustrated by an insufficient number of extrema. From the element with high frequency the IMFs are successively obtained. Hence, the residual signal $res(k)$ has the lowest frequency. Then, for evaluating the imaginary part Hilbert Transform is employed. The Hilbert Transform is used to obtain $Y(t)$ from $X(t)$ as follows

$$Y(t) = \frac{1}{\pi} P \int_{\alpha}^{\alpha} \left(\frac{X(\tau)}{t - \tau} \right) d\tau \tag{14}$$

where P indicates the Cauchy principal values. Then the analytical signal $Z(t)$ is

$$Z(t) = X(t) + iY(t) = \alpha(t)e^{i\theta(t)} \tag{15}$$

where $\alpha(t)$ is the amplitude of $Z(t)$ and $\theta(t)$ is its phase given as follows

$$\alpha(t) = [X^2(t) + Y^2(t)]^{1/2} \tag{16}$$

$$\theta(t) = \arctan \left(\frac{Y(t)}{X(t)} \right) \tag{17}$$

The instantaneous frequency $\omega(t)$ is derived from $\theta(t)$.

$$\omega = \frac{d\theta(t)}{dt} \tag{18}$$

In Hilbert transform, the signal ought to comprise a single frequency or a narrow band of frequencies. The IMF is a narrow band signal. With the Hilbert spectrum already defined, the marginal spectrum $h(\omega)$ can also be defined as follows

$$h(\omega) = \int_0^T H(\omega, t) dt \quad (19)$$

A Spectrum that is calculated using the IMF is called a Hilbert Huang spectrum and it is defined by the following equation.

$$H(t, \omega) = \begin{cases} \alpha(t) & \omega(t) = \omega \\ 0 & \text{otherwise} \end{cases} \quad (20)$$

Here we can generate a Hilbert spectrum contour plot $H(t, \omega)$, which displays the amplitude (z- axis) as the function of time and frequency. The spectrum H is qualitative, but certain integral quantities provide statistics.

As it is mentioned already, the empirical value of SD is using a set within the range (0.2-0.3). Based on the SD , finally the tumor part is segmented from the abnormal BMRI. Selecting the SD range manually is may leads to inaccurate segmentation and hence Particle Swarm Optimization (PSO) is utilized to predict the SD range which leads to get higher accuracy while segmenting the tumor tissues.

3.4.3.2. Selecting SD range with the help of PSO

PSO is a robust optimization technique based on swarm intelligence, which implements the simulation of social behaviour. In the algorithm, each member is seen as a particle and each particle is a potential solution to the problem. In this paper, PSO algorithm is used to select the SD range optimally. The input of the PSO algorithm is SD range. The procedures of PSO algorithm is explained in the following section.

3.4.3.2.1 Steps of PSO algorithm

Initialization

Step 1: The input parameter of PSO algorithm is SD range. Here, initialize the positions and velocity vector of the input parameters randomly. Each parameter is considered as particles, which positions vector is $x_i^k = (x_{i1}^k, x_{i2}^k, \dots, x_{in}^k)$ at iteration k , and velocity vector is $v_i^k = (v_{i1}^k, v_{i2}^k, \dots, v_{in}^k)$ respectively..

Fitness Calculation

Step 2: Evaluate the fitness function of each input parameters.

$$fitness\ function = \max(\text{Point } s) \quad (21)$$

From the abnormal BMRI, a region (I_{Ax}, I_{Ay}) is selected and while applying the SD range, the number of points in that region is counted. The SD range at which maximum points attained are selected as the final SD range.

Based on the fitness function, the optimal SD range is stored and it compares the personal best p_{best}^k of every parameter with its current fitness value. If the current

fitness value is better, then assign the current fitness value to p_{best}^k coordinates. The best solution is achieved by i^{th} particle in iteration k is defined as $P_{besti}^k = (p_{best,1}^k, p_{best,2}^k, \dots, p_{best,n}^k)$. Here, $i=1,2,\dots,n$ and $k=1,2,\dots,d$, which is represents the dimension with specified range.

Step 3: Establish the current best fitness value in the whole inputs. If the current best fitness value is better than global best g_{best} , then assign the current best fitness value to g_{best} and assign the current coordinates to g_{best} coordinates.

Update the position and velocity of input parameter

Step 4: Update the velocity and position of the particles given as in equations (22) and (23).

$$V_i^{k+1} = w * v_i^k + \phi_1 \times rand_1 \times (p_{best_i}^k - x_i^k) + \phi_2 \times rand_2 \times (g_{best}^k - x_i^k) \tag{22}$$

$$X_i^{k+1} = X_i^k + V_i^{k+1} \tag{23}$$

Where, i and ω denotes the particle at i^{th} position and inertia weight. Then ϕ_1 and ϕ_2 are the learning rates governing the particle towards its best position and learning rates governing the social components. The $rand_1$ and $rand_2$ are represented as the random numbers that are uniformly distributed in the range $[0, 1]$. The v_i^k must be specified in the maximum and minimum range of $[v_{max}, v_{min}]$ velocity.

Termination

Step 5: The process is terminated if maximum number of iteration reached or the best SD range is obtained.

The SD range obtained finally is utilized to segment the tumor part separately from the abnormal BMRI. After the segmentation, the segmented tumor part ($t(x, y)$) is utilized to segment the edema tissues in addition to the abnormal BMRI (I_A).

3.4.4. Segmenting Edema Tissues

To segment the edema from the abnormal BMRI, the segmented tumor part ($t(x, y)$) and its corresponding skull stripped abnormal BMRI are utilized as inputs. After gathering the inputs, Histogram Equalization (HE) is applied on the abnormal BMRI in order to enhance the contrast of the abnormal BMRI (I_A). HE adjusts the intensities of the pixel to enhance the contrast of the pixels. Let us take the abnormal BMRI (I_A) in which the intensities of the pixels ranging from 0 to $U-1$. The histogram equalized image (HI_A) is obtained as follow:

$$I_A = floor((U - 1) \sum_{t=0}^{I_{A,x,y}} q_t) \tag{24}$$

$$q_t = \frac{C(t)}{m \times n} \tag{25}$$

Where, $C(t)$ - Count of pixels with intensity t ($t=0, \dots, U-1$) $m' \times n'$ - Total number of pixels

The obtained contrast enhanced image (HI_A) is then converted in to indexed image by means $grayscale()$ which converts the grayscale image in to indexed image using multilevel thresholding. Each pixel in the image is compared with these threshold values to select the pixels.

$$H \rightarrow t_3, S \rightarrow t_4, V \rightarrow t_5$$

$$X = \begin{cases} p_u; p_u \leq t_3, t_5 \& \geq t_4 \\ 0; otherwise \end{cases} \quad (26)$$

Subsequently, the distance is determined between the coordinates of center pixels of the regions in $X_h^{(c)}(x, y)$ and the tumor centroid coordinate value $t(x, y)$.

$$O_h(x, y) = X_h^{(c)}(x, y) - t(x, y) \quad (27)$$

The resultant $O_h(x, y)$ is then verified with threshold value t_6 and an edema region coordinate values are obtained,

$$I_e = \begin{cases} O_h(x, y) \geq t_6 \\ 0; otherwise \end{cases} \quad (28)$$

Then, the morphological dilation and closing operations are performed in the image I_e . The brief description of the edema segmentation process is described in [26]. The image regions are computed by the MATLAB function and the tumor region is selected by the specified threshold value t_7 , the segmented tumor image is represented as I_t . The detailed process of abnormal tissue segmentation is given in [28].

4. Experimental Results and Discussion

The proposed BMRI abnormality detection and tissue segmentation technique is implemented in the working platform of MATLAB (version 2014a) with Intel core i7 Processor, Windows 7 OS, 3.20 GHz CPU Speed and 4 GB RAM. In our work, the given BMRI database has both normal and abnormal Images. To accomplish the tissue segmentation, there is a need to classify the images as normal and abnormal. Correlation and covariance features are extracted from BMRI and given to the FFBNN for the image classification. Fig.4 shows the input BMRI, Skull tripped BMRI, classified normal and abnormal BMRI respectively.

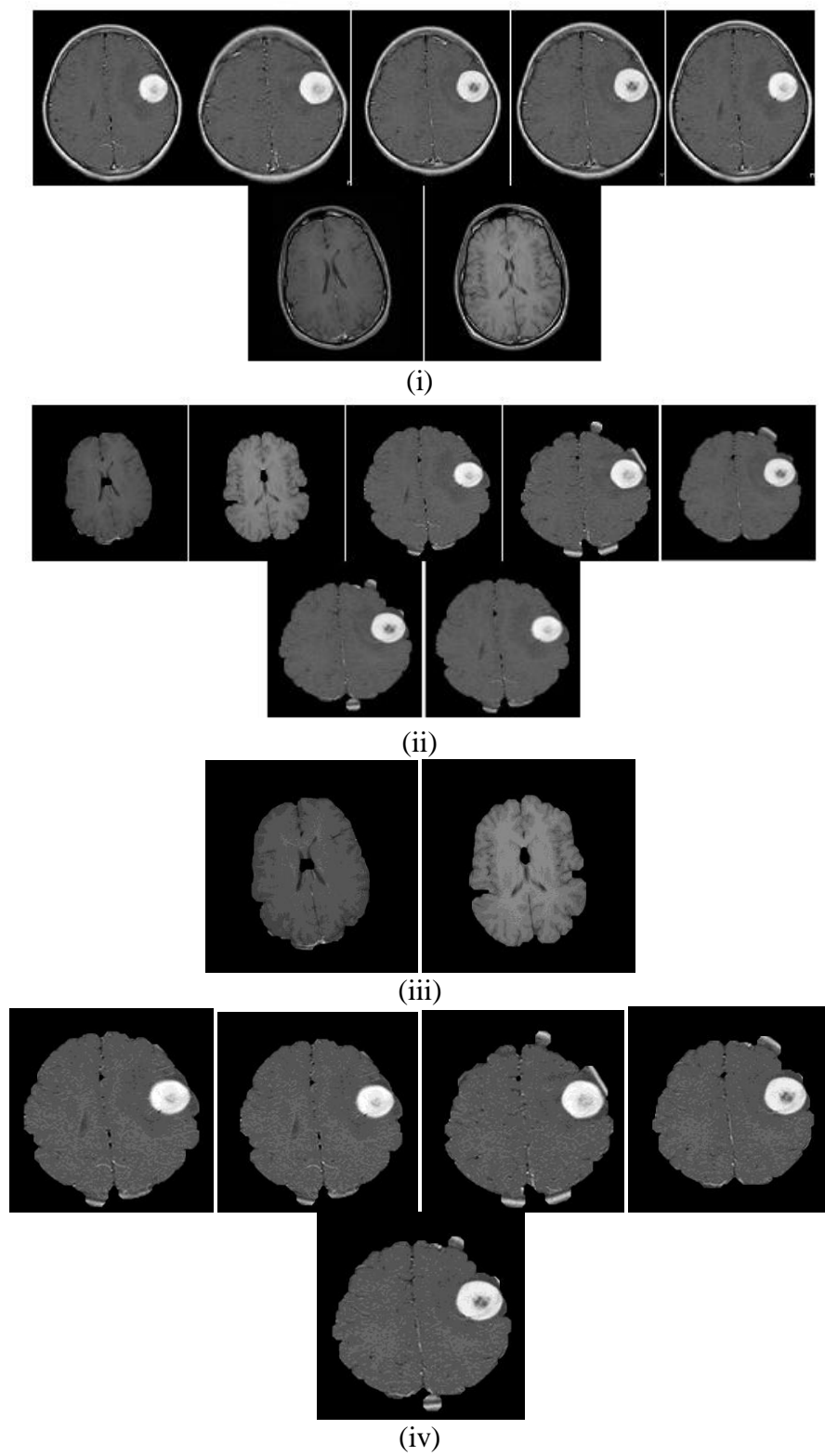


Figure4. (i) Input BMRI, (ii) Skull Stripped BMRI, (iii) Normal BMRI and (iv) Abnormal BMRI

In order to attain efficient classification two familiar classifiers such as Fuzzy and FFBNN are utilized to classify the normal and abnormal BMRI. With the help of the confusion matrix, statistical measures [31] are calculated to evaluate the performance of the proposed technique. Table 1 illustrates the statistical measures of the classifiers used in the proposed technique.

Table1. Classification Performance of the Proposed Technique

Classifier	Accuracy	Sensitivity	Specificity
Fuzzy Logic	100	100	100
FFBNN	85.71	83.33	100

The above table illustrates the classification measurements obtained using the classifiers Fuzzy and FFBNN respectively. By seeing the measurements, it is clearly known that Fuzzy classifier classified the BMRI in an efficient manner than the FFBNN Fuzzy classifier gives 100% accuracy whereas FFBNN gives 85.71% accuracy and similarly for the other metrics, Fuzzy gives higher performance rate than the FFBNN. Hence, classified BMRI obtained using Fuzzy classifier is utilized further for normal and pathological tissues segmentation. To segment the normal tissues like WM and GM, gradient magnitude technique is used and the segmented tissues are shown in Figure 5 (i) and (ii) accordingly. CSF tissues are segmented by means of OPT and it is given in Figure 5 (iii).

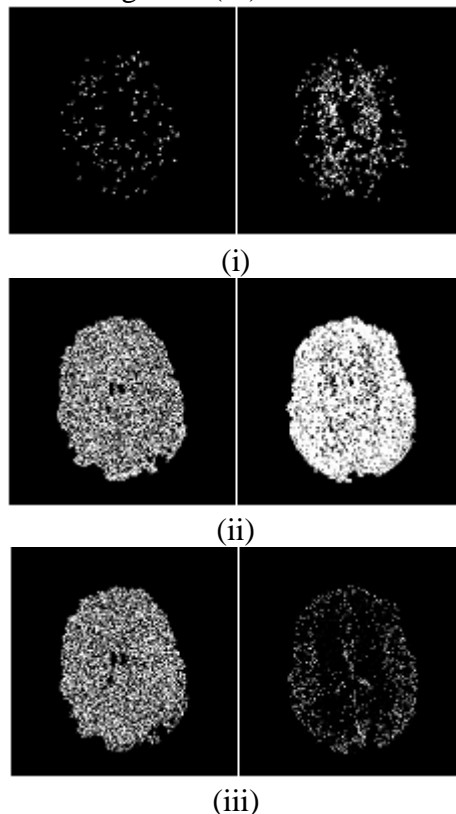




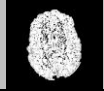
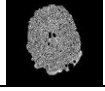
Figure5. Segmented Normal Tissues (i) WM, (ii) GM and (iii) CSF

In the below table 2, performance metrics such as accuracy, sensitivity and specificity for the segmentation of normal tissues like WM, GM and CSF are listed.


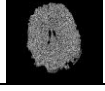
Table2. Normal Tissue Classification Results (i) WM, (ii) GM, (iii) CSF

WM	Accuracy	Sensitivity	Specificity
	94	100	94
	98	85	99

(i)

GM	Accuracy	Sensitivity	Specificity
	96	93	96
	96	95	96

(ii)

CSF	Accuracy	Sensitivity	Specificity
	93	89	96
	95	92	96

(iii)

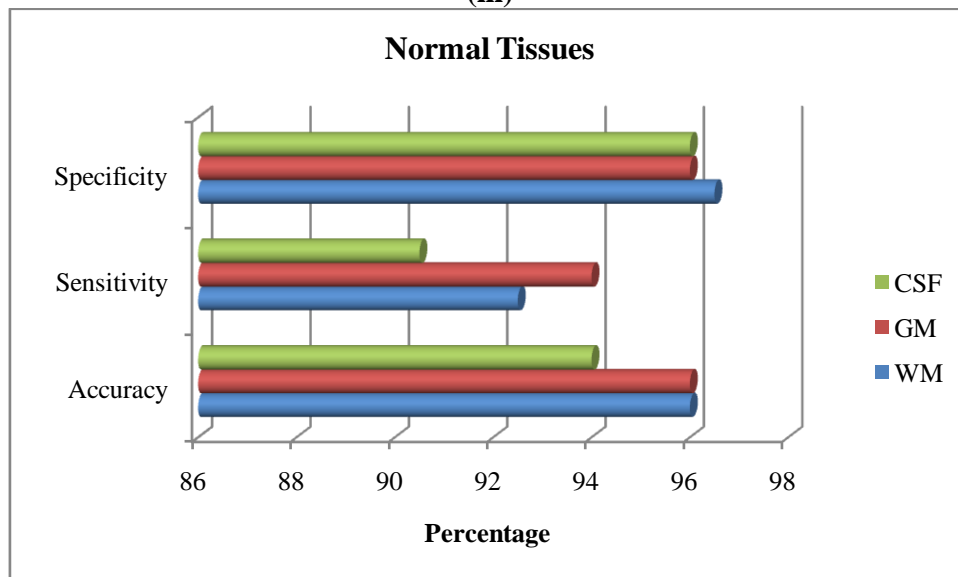


Figure6. Performance measures of Normal Tissues Segmentation in terms of accuracy, sensitivity and specificity

By taking the average of the performance metrics from table 2, figure 6 is drawn. The average accuracy of WM, GM and CSF are 96, 96 and 94; average sensitivity of WM, GM and CSF is 92.5, 94 and 90.5; average specificity of WM, GM and CSF is 96.5, 96 and 96 respectively.

After the classification, the abnormal BMRI is first subjected to tumor tissue segmentation by means of EEHT. While applying EEHT on the abnormal BMRI, Harris edge detector is used to detect the edges given in Figure 7 (i) and Figure 7(ii) shows the tumor parts detected after applying EEHT. The final segmented tumor tissues are shown in figure 7 (iii). After segmenting the tumor tissues, the segmented tumor part and the corresponding abnormal BMRI is subjected to edema tissues segmentation and the resultant edema segmentation images are given in Figure 7 (iv).

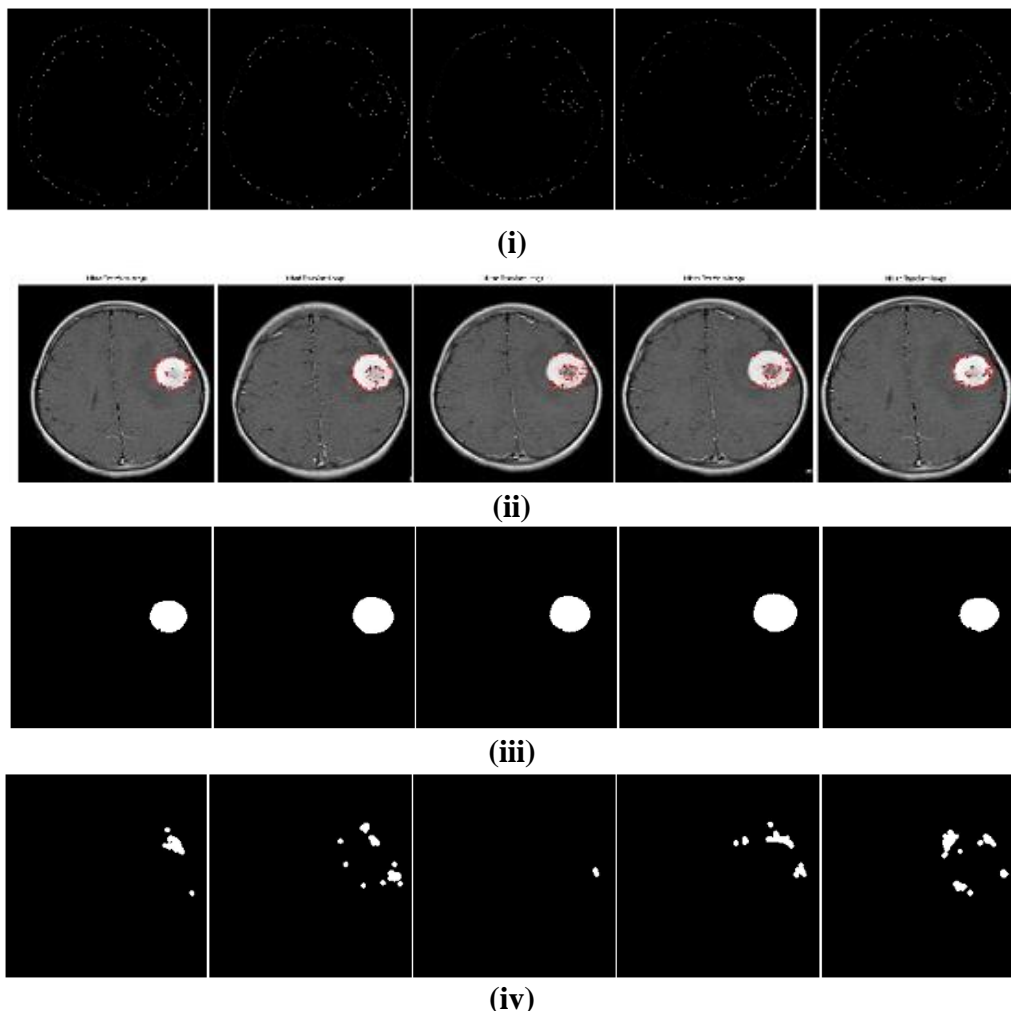

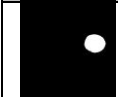
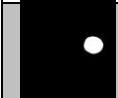
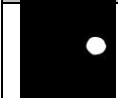
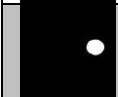







Figure7. Pathological Tissue Segmentation (i) While applying Harris edge detector, (ii) After EEHT, (iii) Tumor Tissues and (iv) Edema Tissues

The proposed pathological tissue segmentation technique is evaluated in terms of accuracy, sensitivity and specificity and listed in table 3.

Table3. Segmentation results in terms of accuracy, sensitivity and specificity (i) tumor and (ii) Edema

Tumor	Accuracy	Sensitivity	Specificity
	97	100	96
	95	92	96
	100	100	100
	92	93	96
	96	95	96

(i)

Edema	Accuracy	Sensitivity	Specificity
	95	100	93
	90	80	93
	97	91	100
	100	100	100
	96	93	96

(ii)

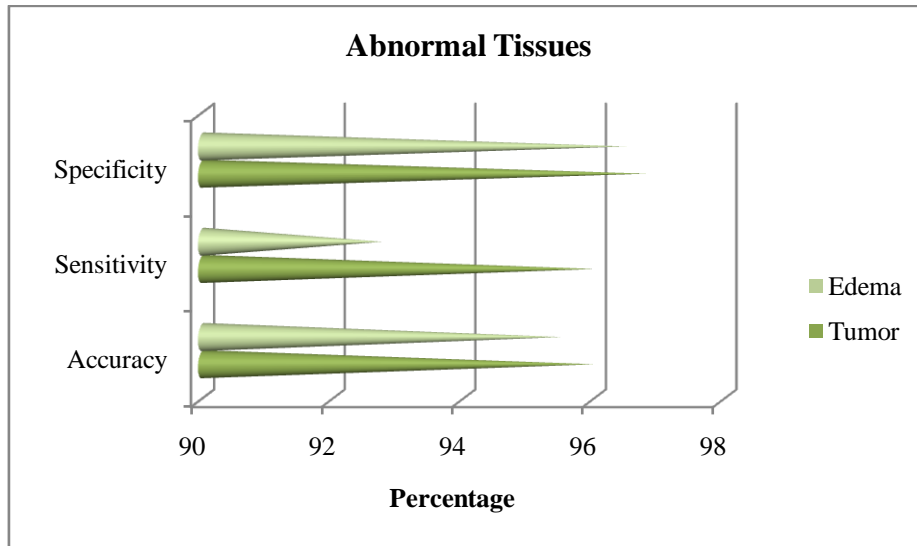


Figure8. Performance measures of Pathological Tissues Segmentation in terms of accuracy, sensitivity and specificity

Figure 8 is drawn by taking the average of the performance metrics from table 3. The average accuracy of Edema and Tumor are 96 and 95.5; average sensitivity of Edema and Tumor is 96 and 92.5; average specificity of Edema and Tumor are 96 and 96.8 respectively.

5. Conclusion

Segmentation of medical imagery is a challenging problem due to the complexity of the images, as well as to the absence of models of the anatomy that fully capture the possible deformations in each structure. The brain is a particularly complex structure, and its segmentation is an important step for many problems, including studies in temporal change detection of morphology, and 3-D visualizations for surgical planning. In this paper, brain abnormality detection and tissue segmentation technique is proposed. FFBNN and Fuzzy Classifier are exploited to classify the BMRI and for segmenting the normal abnormal BMRI tissues 4 various techniques are utilized namely Gradient Magnitude for WM and GM; OPT for CSF; EHHT for Tumor and HE for Edema. The performance of the proposed technique is evaluated in terms of accuracy, sensitivity and specificity. In the normal and abnormal classification, Fuzzy classifier offers better results than the FFBNN. On looking at the tissue segmentation results, the proposed technique yields better performance.

References

1. P. Hagmann, J.-P. Thiran, L. Jonasson et al. DTI mapping of human brain connectivity: statistical fibre tracking and virtual dissection, *NeuroImage*, 2003.
2. M.C. Davidson, K. M. Thomas. and B. J. Casey, "Imaging the developing brain with fMRI", *Mental Retardation and developmental disabilities research reviews*, 2003.
3. V. A. Grau, U. J. Mewes, M. Alcaniz, "Improved watershed transform for medical image segmentation using prior information", *IEEE Trans. on Medical Imaging*, 2004, 23(4): 447-458.
4. H Lv., K. H. Yuan, S. L. Bao, An eSnake model for medical imaging segmentation, *Progress in Natural Science*, 2005.
5. D. L. Pham and J. L. Prince, "Adaptive fuzzy segmentation of magnetic resonance images," *IEEE Trans. Med. Imag.*, 1999.
6. A. F. Goldszal, C. Davatzikos, D. L. Pham, M. X. H. Yan, et al, "An image processing system for qualitative and quantitative volumetric analysis of brain images," *J. Comput. Assist. Tomogra.*, 1998.
7. Arnold J.B., Liow, J.-S., Schaper, K.A., et al., "Qualitative and quantitative evaluation of six algorithms for correcting intensity nonuniformity effects". *NeuroImage*, 2001.
8. R. Moller., R. Zeipelt. "Automatic segmentation of 3D-MRI data using a genetic algorithm, *Medical Imaging and Augmented Reality*", 2001. *Proceedings. International Workshop on*, 10-12 June 2001:278 – 281.
9. W. M.Wells, III,W. E. L. Grimson, R. Kikinis. "Adaptive segmentation of MRI data", *IEEE Trans. Medical Imaging* , 1996.J. C. Bezdek, L.O. Hall, L. P. Clarke, "Review of MR image segmentation techniques using pattern recognition," *Med. Phys.*, vol. 20, No. 4, pp. 1033-1048, 1993.
10. P. Suetens, E. Bellon, D. Vandermeulen, M. Smet, G. Marchal, J. Nuyts, L. Mortelman, "Image segmentation: methods and applications in diagnostic radiology and nuclear medicine," *European Journal of Radiology*, vol. 17, pp. 14-21, 1993.
11. A. Goshtasby, D. A. Turner, "Segmentation of Cardiac Cine MR Images for extraction of right and left ventricular chambers," *IEEE sTrans. Med. Imag.*, vol. 14, No. 1, pp. 56-64, 1995.
12. D. Brzakovic, X. M. Luo, P. Brzakovic, "An approach to automated detection of tumors in mammograms," *IEEE Trans. Med. Imag.*, vol. 9, No. 3, pp. 233-241, 1990.
13. J. F. Brenner, J. M. Lester, W.D. Selles, "Scene segmentation in automated histopathology: techniques evolved from cytology automation," *Pattern Recognition*, vol. 13, pp. 65-77, 1981.
14. K. Lim, A. Pfefferbaum, "Segmentation of MR brain images into cerebrospinal fluid spaces, white and gray matter," *J. Comput. Assist. Tomogr.*, vol. 13, pp. 588-593, 1989.

15. Zhang Y, Brady M, Smith S. "Segmentation of brain MR images through a hidden Markov random field model and expectation-maximization algorithm," *IEEE Trans Med. Imag.*, pp. 45–57, 2001.
16. L. Lemieux, G. Hagemann, K. Krakow, and F. G. Woermann, "Fast, accurate, and reproducible automatic segmentation of the brain in T1-weighted volume MRI data," *Magn. Reson. Med.*, vol. 42, pp. 127–135, 1999.
17. R. Pohle and K. D. Toennies, "Segmentation of medical images using adaptive region growing," *Proc. SPIE— Med. Imag.*, vol. 4322, pp. 1337–1346, 2001.
18. S. Shen, W Sandham, M. Grant and A. Ster, "MRI Fuzzy Segmentation of Brain Tissue Using Neighborhood Attraction with Neural Network Optimization", *IEEE Trans. On Information Technologyis Biomedicine*, vol. 9, No. 3, 2005.
19. Arnaldo Mayer and Hayit Greenspan, "An Adaptive Mean-Shift Framework for MRI Brain Segmentation", *Ieee Transactions On Medical Imaging*, Vol. 28, No. 8, August 2009.
20. Mert R. Sabuncu, B.T. Thomas Yeo, Koen Van Leemput, Bruce Fischl and Polina Golland, "A Generative Model for Image Segmentation Based on Label Fusion", *Ieee Transactions On Medical Imaging*, 2009.
21. Feng Shi, Yong Fan, Songyuan Tang, John H. Gilmore, Weili Lin, Dinggang Shen, "Neonatal brain image segmentation in longitudinal MRI studies", Elsevier Inc., 2009.
22. Juin-Der Lee, Hong-Ren Su, Philip E. Cheng*, Michelle Liou, John A. D. Aston, Arthur C. Tsai, and Cheng-Yu Chen, "MR Image Segmentation Using a Power Transformation Approach", *Ieee Transactions On Medical Imaging*, Vol. 28, No. 6, June 2009.
23. Dalila Cherifi, M.Zinelabidine Doghmane, Amine Nait-Ali , Zakia Aici, Salim Bouzelha, "Abnormal tissus extraction in MRI Brain medical images", *IEEE*, 2011.
24. Nagesh Vadaparathi, Srinivas Yarramalle, Suresh Varma Penumatsa, "Unsupervised Medical Image Segmentation On Brain Mri Images Using Skew Gaussian Distribution", *IEEE-International Conference on Recent Trends in Information Technology, ICRTIT 2011*.
25. K.BALACHANDRAN and DR. R. ANITHA, "An Efficient Optimization Based Lung Cancer Pre-Diagnosis System with Aid of Feed Forward Back Propagation Neural Network (FFBNN)", *Journal of Theoretical and Applied Information Technology*
26. Javeed Hussain, Satya Savithri and Sree Devi, "Segmentation of Tissues in Brain MRI Images using Dynamic Neuro-Fuzzy Technique", *International Journal of Soft Computing and Engineering (IJSCE)*, Vol. 1, No. 6, pp. 416-423, January 2012
27. Nuzhat F. Shaikh and Dharmopal D. Doye, "An Adaptive Iris Recognition System with Aid of Local Histogram and Optimized FFBNN-AAPSO", *International Review on Computers and Softwares*, Vol. 8, No. 12, pp. 2868-2879, 2013

28. Sheejakumari and Ankara Gomathi, "Healthy and Pathological Tissues Classification in MRI Brain Images using Hybrid Genetic Algorithm-Neural Network (HGANN) Approach", *European Journal of Scientific Research*, Vol. 87, No. 2, pp. 212-226, 2012
29. N. E. Huang, Z. Shen, S. R. Long, M. C. Wu, H. H. Shih, Q. Zheng, N. C. Yen, C. C. Tung and H. H. Liu, "The empirical mode decomposition and the Hilbert spectrum for nonlinear and non-stationary time series analysis", In *Proc. of the Royal Society of London. Series A: Mathematical, Physical and Engineering Sciences*, Vol. 454, No. 1971, pp. 903-995, 1998.
30. Naveed ur Rehman and Danilo P. Mandic, "Empirical Mode Decomposition for Trivariate Signals", *IEEE Transactions On Signal Processing*, Vol. 58, No. 3, pp.1059-1068, March 2010.
31. http://en.wikipedia.org/wiki/Sensitivity_and_specificity

